A conserved signaling network monitors delivery of sphingolipids to the plasma membrane in budding yeast

Jesse Clarke[1], Noah Dephoure[2], Ira Horecka[1], Steven Gygi[3], and Douglas Kellogg[1,4]

[1] Department of Molecular, Cell and Developmental Biology, University of California, Santa Cruz, CA 95064

[2] Department of Biochemistry. Weill Cornell Medical College, N.Y. N.Y. 10021

[3] Department of Cell Biology, Harvard Medical School, Boston, MA 02115

[4] Corresponding Author: dkellogg@ucsc.edu.

Character Count (no spaces): 20,570

Abstract

In budding yeast, cell cycle progression and ribosome biogenesis are dependent upon plasma membrane growth, which ensures that events of cell growth are coordinated with each other and with the cell cycle. However, the signals that link the cell cycle and ribosome biogenesis to membrane growth are poorly understood. Here, we used proteome-wide mass spectrometry to systematically discover signals associated with membrane growth. The results suggest that membrane trafficking events required for membrane growth are required for normal sphingolipid-dependent signaling. A conserved signaling network plays an essential role in signaling by responding to delivery of sphingolipids to the plasma membrane. In addition, sphingolipid-dependent signals control protein kinase C (Pkc1), which plays an essential role in the pathways that link the cell cycle and ribosome biogenesis to membrane growth. Together, these discoveries provide new clues to how growth-dependent signaling controls cell growth and the cell cycle.

Introduction

Cell growth is one of the most fundamental features of life, yet remains poorly understood. Growth is the outcome of multiple processes, including ribosome biogenesis and plasma membrane expansion, that must be precisely coordinated. Numerous questions regarding growth remain unanswered: How are plasma membrane growth and ribosome biogenesis coordinated? How is the rate of growth matched to nutrient availability? How is the amount and location of growth during the cell cycle controlled to maintain a constant size and shape?

In budding yeast, entry into mitosis and ribosome biogenesis are dependent upon plasma membrane growth, which could ensure that growth processes are coordinated with each other and with the cell cycle (Li *et al.*, 2000; Nanduri and Tartakoff, 2001; Mizuta and Warner, 1994; Anastasia *et al.*, 2012; McCusker and Kellogg, 2012). The linkage was discovered by analyzing the effects of mutants that block membrane trafficking events required for plasma membrane growth. Thus, inactivation of Sec6, which is required for fusion of vesicles with the plasma membrane, causes an arrest of ribosome biogenesis, as well as a pre-mitotic cell cycle arrest. Both pathways signal via a member of the protein kinase C family (Pkc1) that is localized to sites of membrane growth in the daughter bud. Thus, it is possible that key aspects of cell growth are controlled by common signals originating at sites of membrane growth.

The pathway that links mitotic entry to membrane growth has been proposed to control the amount of polar growth that occurs between bud emergence and entry into mitosis, which would influence both cell size and shape (Anastasia *et al.*, 2012). In this model, the vesicles that drive polar membrane growth are thought to deliver signaling molecules that activate Pkc1. As more vesicles fuse with the plasma membrane, a Pkc1-dependent signal is generated that is proportional to growth, which can be read to determine when sufficient polar growth has occurred. Pkc1 undergoes gradual hyperphosphorylation during polar membrane growth that is dependent upon and proportional to growth, consistent with the idea that it is part of a mechanism that measures polar membrane growth (Anastasia *et al.*, 2012). Growth-dependent signaling suggests a simple and broadly relevant mechanism for control of cell growth and size (McCusker and Kellogg, 2012; Enciso *et al.*, 2014).

The broad outlines of the pathway that links mitotic entry to membrane growth are known. Signaling is dependent upon the Rho1 GTPase, which is delivered to the site of polar growth on vesicles (Abe *et al.*, 2003; Anastasia *et al.*, 2012). Rho1 is activated at the site of growth, where it is thought to bind and control Pkc1 (Kamada et al., 1996; Abe et al., 2003). Pkc1 binds redundant paralogs called Zds1 and Zds2 that recruit PP2A associated with the Cdc55 regulatory subunit ($PP2A^{Cdc55}$). Pkc1 activates $PP2A^{Cdc55}$, which then activates Mih1, the budding yeast homolog of the Cdc25 phosphatase that drives entry into mitosis by removing Cdk1 inhibitory phosphorylation. Activation of mitotic Cdk1 triggers cessation of polar growth and initiation of isotropic growth, which occurs over the entire surface of the bud (Lew and Reed, 1993). Rho1, Pkc1, Zds1/2 and $PP2A^{Cdc55}$ are localized to the site of polar membrane growth and physically interact, providing a direct link between membrane growth and mitotic entry (Yamochi *et al.*, 1994; Kamada *et al.*, 1996; Andrews and Stark, 2000; Rossio and Yoshida, 2011).

A full understanding of how the cell cycle and ribosome biogenesis are linked to membrane growth will require a better understanding of the signals generated at sites of membrane growth. A critical question concerns how membrane growth drives phosphorylation and activation of Pkc1. Previous work suggested that the GTP-bound form of Rho1 generated at sites of growth could play a role (Nonaka *et al.*, 1995; Kamada *et al.*, 1996). However, we have thus far been unable to reconstitute hyperphosphorylation of Pkc1 *in vitro* with purified Rho1-GTP, which suggests that additional signals play a role.

Here, we used proteome-wide mass spectrometry to systematically identify signals associated with membrane growth. To do this, we took advantage of our discovery that Pkc1-dependent signaling rapidly collapses when membrane growth is blocked (Anastasia *et al.*, 2012). Thus, we used proteome-wide mass spectrometry to identify proteins that undergo rapid changes in phosphorylation in response to an arrest of membrane growth.

Results and Discussion

Proteome-wide analysis of signals triggered by an arrest of polarized membrane growth

To identify signals triggered by an arrest of polar membrane growth, we released wild type and *sec6-4* cells from a G1 arrest and shifted to the restrictive temperature during the polar bud growth phase, which corresponds to the interval of bud growth prior to mitotic entry. Samples for mass spectrometry were taken 5 minutes after inactivation of *sec6-4*. Western blotting was used to confirm that the wild type and *sec6-4* cells were at the same point in the cell cycle, and that inactivation of *sec6-4* caused rapid loss of Pkc1 phosphorylation, as previously observed (Anastasia *et al.*, 2012). Proteolytic peptides from each strain were phospho-enriched, covalently modified by reductive dimethylation to generate light (wild type) and heavy (*sec6-4*) stable isotope labeled pools, and then combined and analyzed by LC-MS/MS (Villén and Gygi, 2008; Kettenbach and Gerber, 2011). The heavy to light ratios of phosphorylated peptides in *sec6-4* cells versus wild type cells were $\log_2$ transformed. Thus, negative values indicate decreased phosphorylation in *sec6-4* cells, while positive values indicate increased phosphorylation. Three biological replicates were analyzed, which allowed calculation of average $\log_2$ ratios and standard deviations for most peptides.

The complete data set appears in Tables S1 and S2. Table S1 presents a summary of all identified phosphorylation sites along with quantitative data. Table S2 provides detailed information for each of the detected phosphopeptides. A total of 9375 sites were identified on 1831 proteins. Of these, 6376 sites on 1694 proteins could be quantified.

We focused on sites that were quantified in at least two of the three biological replicates, which comprised 4486 sites on 1519 proteins. We defined a significant change in phosphorylation as a $\log_2$ ratio greater than 1.2 in either direction. At this threshold, 69 sites on 58 proteins underwent rapid dephosphorylation when Sec6 was inactivated (Table S3). 63 sites on 57 proteins showed increased phosphorylation (Table S4). Both Pkc1 and Zds1 underwent significant dephosphorylation in *sec6-4* cells (Table S3). Since these proteins were previously shown to undergo dephosphorylation after inactivation of Sec6, their presence in the data set provides a verification of the approach (Anastasia *et al.*, 2012). Inactivation of Sec6 may cause effects that are independent of its role in membrane growth. For simplicity, however, we refer to the effects of inactivating Sec6 as a block to membrane growth.

Blocking membrane traffic disrupts a signaling network that controls cell growth

We searched the mass spectrometry data for proteins that underwent significant changes in phosphorylation and were previously linked to cell growth. Of particular interest was the protein kinase Ypk1, which showed a loss of phosphorylation. Ypk1, and its paralog Ypk2, are homologs of vertebrate SGK (Casamayor et al., 1999). Extensive work has shown that Ypk1/2, and their surrounding signaling network, play roles in controlling cell growth, lipid synthesis and cell cycle progression. In addition, genetic data suggest that Ypk1/2 control Rho1/Pkc1 signaling (Roelants *et al.*, 2002; Schmelzle *et al.*, 2002).

Figure 1A provides an overview of the Ypk1/2 network, with proteins identified by mass spectrometry highlighted in red. One function of the network is to modulate synthesis of sphingolipids, a diverse family of lipids that includes major components of the plasma membrane, as well as lipids that play roles in signaling (Roelants *et al.*, 2011). Sphingolipid synthesis is initiated at the endoplasmic reticulum by serine palmitoyltransferase (SPT), which synthesizes precursors for production of phytosphingosine and ceramides, which are used to produce complex sphingolipids in the Golgi. Complex sphingolipids are transported to the plasma membrane and together constitute approximately 10% of membrane lipids (Klose et al., 2012). Ypk1/2 promote sphingolipid synthesis by phosphorylating and inhibiting Orm1 and Orm2, redundant paralogs that bind and inhibit serine palmitoyltransferase (Breslow *et al.*, 2010; Roelants *et al.*, 2011).

Ypk1/2 are phosphorylated by a pair of redundant kinase paralogs called Fpk1 and Fpk2 that localize to the site of polar growth (Nakano *et al.*, 2008; Roelants *et al.*, 2010). Genetic data suggest that complex sphingolipids are required for Fpk1/2 activity, and that Fpk1/2 inhibit Ypk1/2. Fpk1/2 also phosphorylate a redundant pair of lipid flippases called Dnf1 and Dnf2, which are located at the site of polar growth and are thought to flip phospholipids from the outer to inner leaflet of the plasma membrane (Hua *et al.*, 2002; Pomorski *et al.*, 2003; Nakano *et al.*, 2008). Loss of *FPK1/2* or *DNF1/2* causes mild elongation of the daughter bud, which suggests that they play a role in controlling polar growth (Pomorski *et al.*, 2003; Nakano *et al.*, 2008).

The key upstream kinases that control Ypk1/2 are target of rapamycin complex 2 (TORC2), and phosphoinositide-dependent kinase 1 (PDK1), which play conserved roles in controlling cell growth (Roelants *et al.*, 2002; Kamada *et al.*, 2005). In budding yeast, PDK1 is encoded by redundant paralogs called *PKH1* and *PKH2*. TORC2 and Pkh1/2 phosphorylate distinct sites on Ypk1/2 that are thought to increase activity.

Blocking membrane traffic causes reduced sphingolipid-dependent signaling

Multiple proteins in the Ypk1/2 signaling network underwent significant changes in phosphorylation in response to inactivation of Sec6, including Ypk1, Orm2, Dnf2 and Avo1, a component of the TORC2 complex. All of these proteins regulate and/or respond to sphingolipids. To further investigate changes in the Ypk1/2 signaling network, we first analyzed phosphorylation of Ypk1. Fpk1/2-dependent phosphorylation of Ypk1 causes a decrease in electrophoretic mobility that can be detected by western blotting (Roelants et al., 2011). Inactivation of Sec6 caused loss of Fpk1/2-dependent phosphorylation of Ypk1, which suggests that blocking membrane traffic causes inactivation of Fpk1/2 (Figure 1B). The fact that Dnf2, a direct target of Fpk1/2, showed the largest loss of phosphorylation in the data set provided further evidence for a loss of Fpk1/2 activity. Since Fpk1/2 are dependent upon complex sphingolipids, the loss of Fpk1/2 activity suggests that inactivation of Sec6 causes a decrease in sphingolipid-dependent signaling. Addition of exogenous phytosphingosine rescued the loss of Ypk1 phosphorylation, consistent with the idea that inactivation of Sec6 causes loss of sphingolipid-dependent signals (Figure 1C). The rescue was transient, which suggests that the relevant signaling lipids are short-lived or rapidly transported to a location where they can not influence Fpk1/2 activity.

The site on Orm2 that was detected was previously identified as a likely Ypk1/2 target (Breslow *et al.*, 2010; Roelants *et al.*, 2010; 2011). The mass spectrometry data suggested that Orm2 is dephosphorylated when Sec6 is inactivated. To investigate further, we used Phos-tag gels and western blotting to assay Orm2 phosphorylation after inactivation of Sec6. In contrast to expectations from the mass spectrometry data, Orm2 became rapidly hyperphosphorylated when Sec6 was inactivated, which indicates that Ypk1/2 become more active (Figure 1D). The disagreement between the mass spectrometry and western blotting data may be a product of the complexity of phosphopeptide analysis. Phosphosites on Orm1/2 are located close to each other,

such that multiple sites are found on the same proteolytic peptide. If a singly phosphorylated peptide is converted to a multiply phosphorylated peptide upon inactivation of Sec6, the analysis will detect a decrease in the abundance of the singly phosphorylated peptide, giving the appearance of a dephosphorylation event.

Since the Orm1/2 proteins are embedded in the membrane of the endoplasmic reticulum (Han et al., 2010), the discovery that they undergo rapid hyperphosphorylation in response to an arrest of plasma membrane growth suggests that there is rapid communication between the plasma membrane and the endoplasmic reticulum. Approximately 50% of the endoplasmic reticulum is closely associated with the plasma membrane, which would facilitate rapid communication (Pichler et al., 2001).

The mass spectrometry also found that Avo1, a component of the TORC2 complex, undergoes increased phosphorylation in response to an arrest of membrane growth (Table S4). Since Avo1 is a target of TORC2, this observation suggests that TORC2 activity increases (Wullschleger *et al.*, 2005). To test this, we assayed TORC2-dependent phosphorylation of Ypk1 using a phosphospecific antibody (Figure 1E). Inactivation of Sec6 caused increased TORC2-dependent phosphorylation of Ypk1. We again observed that inactivation of Sec6 caused loss of the Fpk1/2-dependent mobility shift of Ypk1.

Previous work found that inhibition of the first step of sphingolipid synthesis causes inactivation of Fpk1/2, activation of TORC2 and Ypk1/2, and hyperphosphorylation of Orm1/2 (Breslow *et al.*, 2010; Roelants *et al.*, 2011; Sun *et al.*, 2012). Since hyperphosphorylation of Orm1/2 relieves inhibition of sphingolipid synthesis, the network was proposed to be responsible for homeostatic control of sphingolipid synthesis (Breslow *et al.*, 2010). Here, we found that blocking transport of lipids to the plasma membrane causes effects identical to those caused by inhibition of sphingolipid synthesis. This discovery demonstrates that blocking membrane growth causes an abrupt loss of sphingolipid-dependent signals. In addition, although inactivation of Sec6 caused hyperphosphorylation of Orm2, which should stimulate sphingolipid synthesis at the endoplasmic reticulum, there was no evidence that increased sphingolipid synthesis was perceived by the network: TORC2-dependent phosphorylation of Ypk1/2 persisted, Fpk1/2 remained inactive, and Orm2 phosphorylation persisted. Together, these observations suggest that the signaling network measures transport of sphingolipids to the plasma membrane, rather than synthesis of sphingolipids at the endoplasmic reticulum. A model that could explain the data is that post-Golgi vesicles required for polar growth deliver sphingolipids to the plasma membrane. When vesicle delivery is blocked, sphingolipids at the plasma membrane rapidly decline, which could occur by modification or sequestration into lipid domains. Loss of sphingolipids, in turn, would lead to inactivation of Fpk1/2 and a consequent loss of Ypk1/2 and Dnf1/2 phosphorylation. A decrease in sphingolipids would also cause increased activity of TORC2, which stimulates Ypk1/2 to hyperphosphorylate Orm1/2.

Inactivation of Ypk1/2 causes a failure in Pkc1 phosphorylation that is rescued by exogenous sphingolipids

We next tested whether Ypk1/2 are required for normal control of Pkc1. We utilized an analog-sensitive allele of *YPK1* in a *ypk2Δ* background (*ypk1-as ypk2Δ*), which allowed rapid inactivation of Ypk1/2 with the inhibitor 3-MOB-PP1 (Sun et al., 2012). Addition of 3-MOB-PP1 to wild type cells prior to bud emergence had no effect on Pkc1 phosphorylation or bud emergence. It also had no effect on mitotic entry, as assayed by accumulation of the mitotic cyclin Clb2 (Figure 2A, B). In contrast, addition of inhibitor to *ypk1-as ypk2Δ* cells caused a failure in Pkc1 hyperphosphorylation, as well as delayed bud emergence and delayed synthesis of mitotic cyclin. The fact that bud emergence and mitotic cyclin synthesis still occurred when Ypk1/2 were

inhibited indicated that the failure in Pkc1 phosphorylation was not due simply to failures in bud growth or mitotic entry (Figure 2C).

To determine whether the delay in bud emergence was due to decreased Pkc1 activity, we expressed a constitutively active version of *PKC1* (*PKC1**) in *ypk1-as ypk2Δ* cells (Watanabe et al., 1994). We used basal expression from the uninduced *CUP1* promoter to achieve low level expression of *PKC1** (Thai *et al.*, 2017). Expression of *PKC1** rescued the delay in bud emergence (Figure 2B, C). Together, these observations suggest that inhibition of Ypk1/2 causes decreased phosphorylation of Pkc1, as well as decreased Pkc1 activity.

Inhibition of Ypk1/2 should lead to decreased synthesis of sphingolipids due to hyperactivity of Orm1/2 (Figure 1A) (Breslow *et al.*, 2010; Roelants *et al.*, 2011; Sun *et al.*, 2012). We therefore added exogenous phytosphingosine to test whether failure to phosphorylate Pkc1 when Ypk1/2 are inhibited is a consequence of decreased sphingolipid production. Addition of phytosphingosine largely restored hyperphosphorylation of Pkc1 when Ypk1/2 were inhibited, although Pkc1 phosphorylation was slightly delayed (Figure 3A, compare the fraction of Pkc1 that reaches the fully hyperphosphorylated form). We further discovered that expression of constitutively active *PKC1** suppressed lethality caused by myriocin, a compound that inhibits serine palmitoyltransferase and causes a reduction in sphingolipids (Figure 3B) (Sun et al., 2000). This observation provides further evidence that Pkc1 is downstream of sphingolipid-dependent signals.

The buds that emerged during Ypk1/2 inhibition were elongated (Figure 3C and Supplemental Figure S1). Cell elongation was quantified by measuring the average ratio of bud length to width (Figure 3D). Addition of phytosphingosine largely eliminated the elongated bud phenotype (Figure 3B, C). Previous studies showed that bud elongation can be a consequence of decreased activity of Pkc1 or mitotic Cdk1 (Lew and Reed, 1993; Anastasia *et al.*, 2012).

Sphingolipids are also thought to regulate Pkh1/2, which directly phosphorylate Pkc1 on a site that stimulates its activity (Inagaki *et al.*, 1999; Sun *et al.*, 2000; Friant *et al.*, 2001; Roelants *et al.*, 2004; Liu *et al.*, 2005). Since Pkh1/2 phosphorylate Pkc1 on a single site, they are unlikely to be directly responsible for the gradual multi-site hyperphosphorylation of Pkc1 that occurs during polar membrane growth. However, Pkh1/2 could activate Pkc1 to undergo autophosphorylation. To test the contribution of Pkh1/2, we utilized an analog-sensitive allele of *PKH1* in a *pkh2Δ* background (*pkh1-as pkh2Δ*) (Sun et al., 2012). Inactivation of Pkh1/2 caused a rapid and complete loss of Pkh1/2-dependent phosphorylation of Ypk1, as revealed by a phosphospecific antibody (Figure 4A). However, it did not cause a loss of Pkc1 phosphorylation, which indicates that dephosphorylation of Pkc1 in response to an arrest of membrane growth is not likely to be caused by loss of Pkh1/2 activity (Figure 4A).

Addition of exogenous phytosphingosine did not rescue the loss of Pkc1 phosphorylation caused by inactivation of Sec6 (Figure 4B). This suggests that vesicle traffic from the Golgi to the plasma membrane is required for sphingolipids to influence Pkc1 phosphorylation.

Inhibition of sphingolipid production causes reduced phosphorylation of Pkc1

To further define the contribution of sphingolipids, we utilized a temperature sensitive allele of *LCB1* (*lcb1-100*), which encodes an essential subunit of serine palmitoyltransferase (Meier et al., 2006). Inactivation of Lcb1 caused a decrease in Pkc1 hyperphosphorylation during polar growth, which could be seen as a failure to produce significant amounts of the most hyperphosphorylated forms of Pkc1 (Figure 4C). Analysis of mitotic cyclin levels revealed that inactivation of Lcb1 also caused delayed mitotic entry and a prolonged mitosis (Figure 5A). Cells budded when Lcb1 was inactivated so the delay was not due to a failure in bud growth (not shown). Addition of exogenous phytosphingosine largely rescued Pkc1 hyperphosphorylation and the mitotic delay, which suggests that the effects of *lcb1-100* were due to a failure to produce

sphingolipids (Figure 5A). A previous study found additional evidence for sphingolipid-dependent control of Pkc1. In this case, it was found that blocking production of sphingolipids causes a failure in endocytosis that is rescued by overexpression of Pkc1 (Friant *et al*., 2000).

Together, the data indicate that an arrest of membrane growth causes an abrupt decrease in sphingolipid-dependent signals. The data further suggest that the Ypk1/2 signaling network monitors vesicle-dependent transport of sphingolipids to the plasma membrane, rather than synthesis of sphingolipids at the endoplasmic reticulum. Finally, the data suggest that delivery of sphingolipids to the plasma membrane plays a role in controlling Pkc1, which functions in the signaling pathways that link cell cycle progression and ribosome biogenesis to membrane growth.

An intriguing interpretation of the data is that the sphingolipid signaling network functions to coordinate aspects of cell growth. The network constitutes a feedback loop in which sphingolipids control the activities of TORC2 and Ypk1/2, while TORC2 and Ypk1/2 control production of sphingolipids. Sphingolipids are precursors for synthesis of major components of the plasma membrane. Thus, the feedback loop could help ensure that growth of the plasma membrane is coordinated with synthesis of precursors at the endoplasmic reticulum. Since TORC2 and Ypk1/2 are also thought to control diverse aspects of cell growth, the feedback loop could work more broadly to coordinate events of cell growth. Moreover, since the TORC complexes relay signals regarding nutrient availability, TORC2-dependent modulation of the network could ensure that the rate of plasma membrane growth is matched to the growth rate set by nutrients. A previous study found that myriocin, an inhibitor of the first step in sphingolipid synthesis, causes a dose dependent hyperphosphorylation of the Orm1/2 proteins. This observation suggests that the signaling network can measure the amount of sphingolipids transported to the plasma membrane, rather than simply measuring whether they are being transported. In this case, the network could generate signals that are proportional to the amount of sphingolipids transported to the plasma membrane. This kind of proportional growth signal could be used to measure and control cell size. Indeed, the data suggest that growth-dependent phosphorylation of Pkc1 may be dependent upon signals from sphingolipids.

The mechanism by which sphingolipids are sensed remains mysterious. Protein binding sites for sphingolipids, which would presumably be required for sensing, have not been identified in budding yeast. The location at which sphingolipids are sensed is also uncertain. The data suggest that sensing occurs at the plasma membrane; however, it remains possible that sphingolipids at the plasma membrane are internalized by endocytosis and detected at internal membranes.

The idea that cell growth and size are controlled by lipid-dependent signals is appealing. Control of cell growth and size would have been essential for survival of the earliest cells, so it is likely that the underlying mechanisms are ancient and conserved. Membranes that allow compartmentalization are one of the most fundamental and conserved features of cells, so it would make sense that mechanisms that control membrane growth evolved early and in close association with membrane lipids. Overall, we have a surprisingly limited understanding of the mechanisms and regulation of membrane growth during the cell cycle. A full understanding of cell growth, and the mechanisms that limit growth to control cell size, will require a deeper understanding of these mechanisms.

Materials and Methods

Yeast strains, culture conditions and plasmids

Most strains used in this study are in the W303 strain background (*leu2-3,112 ura3-1 can1-100 ade2-1 his3-11,15 trp1-1 GAL+ ssd1-d2*), except for DDY903 and YSY1269, which are in the S288C background (*his3-Δ200 leu2-3, 112, ura3-52*). The additional features of the strains used this study are listed in Table S5. Cells were grown in YEPD media (1% yeast extract, 2% peptone, 2% dextrose) supplemented with 40 mg/L adenine, or in YEP media (1% yeast extract, 2% peptone) supplemented with 40 mg/L adenine and with different carbon sources, as noted.

One-step PCR-based gene replacement was used for making deletions and adding epitope tags at the endogenous locus (oligonucleotide sequences available upon request) (Longtine et al., 1998; Janke et al., 2004). To make a strain that expresses an analog-sensitive allele of *PKH1*, the *PKH1* gene was amplified and cloned into vector pRS306 (URA3). Site directed mutagenesis was then used to introduce mutations L203A and F187V to make plasmid pJZ5A (*pkh1-as, URA3*), as previously described (Sun et al., 2012). DK2547 was made by digesting plasmid pJZ5A with MscI to target integration at the *PKH1* locus in *pkh2Δ* cells. After selection for plasmid integration, recombination events that loop out the plasmid were selected on FOA, and sequencing was used to identify looping out events that left the mutants behind. DK2876 was constructed similarly by digesting the vector pRS306-YPK1-as (*ypk1-L424A URA3)* with AflII, and integrating at YPK1 in *ypk2Δ* cells, followed by selection on URA3 and subsequent selection on FOA (Sun et al., 2012).

Cell cycle time courses

To synchronize cells in G1 phase, cells were grown overnight to log phase in YEPD at room temperature. Cells at an OD_{600} of 0.6 were arrested in G1 by addition of alpha factor to 0.5 μg/ml (bar1- strains) or 15 μg/ml (BAR+ strains). Cells were arrested at room temperature for 3.5 hours and released by washing 3X with fresh YEPD. Time courses were carried out at 25ºC unless otherwise noted. To prevent cells from re-entering the cell cycle, alpha factor was added back at 90 minutes after release from arrest. For time courses using analog-sensitive alleles, the cells were grown in YEPD media without supplemental adenine.

Western blotting

To prepare samples for western blotting, 1.6 ml of culture were collected and centrifuged at 13000 rpm for 30s. The supernatant was removed and 250 μl of glass beads were added before freezing in liquid nitrogen. Cells were lysed by bead-beating in 140μl of 1X sample buffer (65 mM Tris-HCl, pH 6.8, 3% SDS, 10% glycerol, 50 mM NaF, 100 mM beta-glycerolphosphate, 5% 2-mercaptoethanol, 2 mM phenylmethylsulfonyl fluoride (PMSF) and bromophenol blue). The PMSF was added immediately before lysis from a 100 mM stock in ethanol. Cells were lysed in a mini-beadbeater-16 (Biospec Products) at top speed for 2 minutes. The samples were then centrifuged for 15 seconds at 13000 rpm, placed in boiling water bath for 5 min, and centrifuged for 5 min at 13000 rpm. SDS-PAGE was carried out as previously described using a 10% acrylamide gel (Harvey et al., 2005). Gels were run at a constant current of 20 mA until a prestained molecular weight marker of 57.6 kD was near the bottom of the gel.

For western blotting, protein was transferred to nitrocellulose membranes (or PVDF membranes for Pkc1 probing) for 1h 30min at 800 mA at 4ºC in a Hoeffer transfer tank in buffer containing 20 mM Tris base, 150 mM glycine, and 20% methanol. Blots were probed overnight at room temperature with affinity-purified rabbit polyclonal antibodies raised against Pkc1, Clb2, or HA peptide (Anastasia *et al.*, 2012). Anti-FLAG rabbit polyclonal antibody was from Sigma-Aldrich. TORC2-dependent phosphorylation of Ypk1 was detected using rabbit polyclonal anti-

phospho-Ypk1(T662) (Gift of Ted Powers) and Pkh1/2-dependent phoshorylation of Ypk1 and Ypk2 was detected using a phospho-specific antibody that recognizes Ypk1 phosphorylated at T504 (Santa Cruz Biotechnology, Dallas, TX; Catalog number: sc-16744 P).

PhosTag™ gels were used to resolve phosphorylated forms of Orm2-Flag (Kinoshita et al., 2006). Samples were loaded onto 10% polyacrylamide gels containing 50 µM Phos-tag (Wako Chemicals USA, Richmond, VA) and 100 µM $MnCl_2$. Gels were rinsed twice for 10 min in transfer buffer containing 2 mM EDTA. Gels were transferred to nitrocellulose using the Trans-Blot® Turbo™ transfer system (BioRad USA, Hercules, CA).

Analysis of bud emergence and polarity

To analyze bud emergence and polarity, samples from synchronized cultures were fixed with 3.7% formaldehyde and analyzed by light microscopy or by immunofluorescence, as previously described (Pringle et al., 1991). Bud polarity was analyzed in samples taken 120 minutes after release from G1 phase arrest. ImageJ was used to measure bud length and width, and the ratio was averaged for at least 50 cells in each sample. The average length and width of each strain were depicted as ovals (lines represent standard error) included with the bar graph whose relative shape and size can be directly compared.

Preparation of samples for mass spectrometry

To prepare samples for mass spectrometry, wild type and *sec6-4* cells were grown in YEPD medium overnight at room temperature to an optical density of $O.D._{600}$ 0.8. Cells were arrested in G1 with mating pheromone and released from the arrest at room temperature. At 70 minutes after release from the G1 arrest, cells were shifted to a 34ºC water bath and samples for mass spectrometry were taken 5 minutes after the shift. Samples for western blotting were collected before and after the shift to confirm that Pkc1 underwent dephosphorylation.

For each sample, 50 ml of cells were harvested by centrifuging 1 minute at 3800 rpm. The cells were resuspended in 1 ml YPD and transferred to a 2 ml screw-top tube. The cells were pelleted for 30 seconds, the supernatant was removed, and 250 ul of glass beads were added before freezing the cells on liquid nitrogen. All tubes, centrifuge buckets, and media were pre-warmed to 34ºC to maintain restrictive temperature during cell collection.

To lyse the cells, 500 µl of ice cold lysis buffer (8 M urea, 75 mM NaCl, 50 mM Tris-HCl pH 8.0, 50 mM NaF, 50 mM ß-glycerophosphate, 1 mM sodium orthovanadate, 10 mM sodium pyrophosphate, 1 mM PMSF) were added to the harvested cells before lysis using a Biospec Multibeater-16 at top speed for three cycles of 1 min, each followed by a 1 min incubation on ice to avoid over-heating. Samples were centrifuged at 13000 rpm for 10 minutes at 4ºC and the lysates were transferred to fresh 1.6 ml tubes and spun again before transferring to new 1.6 ml tubes. A 5 µL aliquot was taken from each sample for Bradford assay and protein quantification before flash freezing in liquid nitrogen. Three biological replicates for each strain were collected and analyzed by mass spectrometry.

Disulfide bonds were reduced by adding dithiothreitol to a final concentration of 2.5 mM and incubating at 56°C for 40 min. The extract was allowed to cool to room temperature and the reduced cysteines were alkylated by adding iodoacetamide to 7.5 mM and incubating for 40 min in the dark at room temperature. Alkylation was quenched with an additional 5 mM dithiothreitol. Peptide digestion and labeling by reductive dimethylation were carried out as previously described (Zapata et al., 2014).

Phosphopeptide enrichment by SCX/TiO2

Phosphopeptides were enriched using a modified version of the two-step, SCX-IMAC/TiO_2 protocol employing step elution from self-packed solid-phase extraction strong cation exchange

(SCX) chromatography cartridges as previously described with some changes (Villén and Gygi, 2008). Peptides were resuspended in 1 ml SCX buffer A (7 mM KH_2PO_4, pH 2.65, 30% ACN) and loaded onto pre-equilibrated syringe-barrel columns packed with 500 mg of 20 μm, 300 Å, polysulfoethylA resin (poly LC). The loading flow-through was collected and pooled with a 2 ml wash with buffer A. Seven additional fractions were collected after sequential addition of 3 ml of SCX buffer A containing increasing concentrations of KCl; 10, 20, 30, 40, 50, 60 and 100 mM KCl. All fractions were frozen in liquid nitrogen, lyophilized, resuspended in 1 ml of 1% FA, and desalted on 50 mg Sep-paks. Peptides were eluted with 500 μl of 70% ACN, 1% FA. Five percent of each fraction was taken off for protein abundance analysis. The remaining peptides were dried in a speed vac. TiO_2 enrichment was performed as in (Kettenbach and Gerber, 2011). Dried peptides were resuspended in 300 μl wash/binding buffer (50% ACN, 2 M lactic acid) and incubated with 90 mg of prewashed Titansphere TiO_2 beads (GL Sciences, #5020-75000) with vigorous shaking for 60 minutes at room temperature. The beads were washed two times with 300 μl of wash/binding buffer and then two times with 300 ul 50% ACN/1% FA. Phosphopeptides were eluted in two steps by sequential treatments with 75 μl 50 M KH_2PO_4, pH 10.7. The eluates were acidified by the addition of FA to 2% final concentration, desalted on STAGE tips (Rappsilber et al., 2003), and dried in a speed vac. Eight fractions were analyzed by LC-MS/MS.

Mass spectrometry

Phosphopeptide samples were analyzed on a LTQ Orbitrap Velos mass spectrometer (Thermo Fisher Scientific) equipped with an Accela 600 quaternary pump (Thermo Fisher Scientific) and a Famos microautosampler (LC Packings, Sunnyvale, CA). Nanospray tips were hand-pulled using 100 µm I.D. fused-silica tubing and packed with 0.5 cm of Magic C4 resin (5µm, 100 Å, Michrom Bioresources, Auburn, CA) followed by 20 cm of Maccel C18AQ resin (3µm, 200 Å, Nest Group, Southborough, MA). Peptides were separated using a gradient of 3% to 28% ACN in 0.125% FA over 70 min with an in column flow rate of ~300-500 nl/min.

Peptides were detected using a data-dependent Top20-MS2 method. For each cycle, one full MS scan of m/z = 300-1500 was acquired in the Orbitrap at a resolution of 60,000 at m/z = 400 with AGC target = $1x10^6$ and maximum ion accumulation time of 500 mS. Each full scan was followed by the selection of the most intense ions, up to 20, for collision induced dissociation (CID) and MS2 analysis in the LTQ. An AGC target of $2x10^3$ and maximum ion accumulation time of 150 mS was used for MS2 scans. Ions selected for MS2 analysis were excluded from re-analysis for 60 sec. Precursor ions with charge = 1+ or unassigned were excluded from selection for MS2 analysis. Lockmass, employing atmospheric polydimethylsiloxane (m/z = 445.120025) as an internal standard was used in all runs to calibrate orbitrap MS precursor masses. Each sample was analyzed twice for a total of 48 runs.

Peptide identification and filtering

MS2 spectra were searched using SEQUEST v.28 (rev. 13) (Eng et al., 1994) against a composite database containing the translated sequences of all predicted open reading frames of *Saccharomyces cerevisiae* (http://downloads.yeastgenome.org, downloaded 10/30/2009) and its reversed complement, using the following parameters: a precursor mass tolerance of ±20 ppm; 1.0 Da product ion mass tolerance; lysC digestion; up to two missed cleavages; static modifications of carbamidomethylation on cysteine (+57.0214), dimethyl adducts (+28.0313) on lysine and peptide amino termini; and dynamic modifications for methionine oxidation (+15.9949), heavy dimethylation (+6.0377) on lysine and peptide amino termini, and phosphate (+79.9663) on serine, threonine, and tyrosine for phosphopeptide enriched samples.

Peptide spectral matches were filtered to 1% FDR using the target-decoy strategy (Elias and Gygi, 2007) combined with linear discriminant analysis (LDA) (Huttlin et al., 2010) using

several different parameters including Xcorr, ΔCn', precursor mass error, observed ion charge state, and predicted solution charge state. Linear discriminant models were calculated for each LC-MS/MS run using peptide matches to forward and reversed protein sequences as positive and negative training data. Peptide spectral matches within each run were sorted in descending order by discriminant score and filtered to a 1% FDR as revealed by the number of decoy sequences remaining in the data set. The data were further filtered to control protein level FDRs. Peptides from all fractions in each experiment were combined and assembled into proteins. Protein scores were derived from the product of all LDA peptide probabilities, sorted by rank, and filtered to 1% FDR as described for peptides. The FDR of the remaining peptides fell dramatically after protein filtering. Remaining peptide matches to the decoy database were removed from the final dataset.

For inclusion in quantitative calculations, peptides were required to have a minimum signal-to-noise ratio of ≥ 5 or a maximum value ≥ 10 for heavy and light species. Ratios were normalized to recenter the distribution at 1:1 ($\log_2 = 0$). Phosphorylation site ratios were calculated from the median of all quantified phosphopeptides harboring each site in each replicate.

Phosphorylation site localization analysis was done using the Ascore algorithm (Beausoleil et al., 2006). These values appear in Tables S1 and S2.

Acknowledgements

We thank Ted Powers for the anti-phospho-Ypk1(T662P) antibody. We also thank Yidi Sun and David Drubin for helpful advice and sharing strains, members of the Kellogg laboratory for advice and critical reading of the manuscript, and Ben Abrams and the UCSC Life Sciences Microscopy Center for assistance with microscopy. This work was supported by the NIH Grant GM109143.

Competing Interests

The authors have no competing interests.

References

Abe, M., Qadota, H., Hirata, A., and Ohya, Y. (2003). Lack of GTP-bound Rho1p in secretory vesicles of Saccharomyces cerevisiae. The Journal of Cell Biology *162*, 85–97.

Anastasia, S. D., Nguyen, D. L., Thai, V., Meloy, M., MacDonough, T., and Kellogg, D. R. (2012). A link between mitotic entry and membrane growth suggests a novel model for cell size control. The Journal of Cell Biology *197*, 89–104.

Andrews, P. D., and Stark, M. J. (2000). Dynamic, Rho1p-dependent localization of Pkc1p to sites of polarized growth. Journal of Cell Science *113 (Pt 15)*, 2685–2693.

Breslow, D. K., Collins, S. R., Bodenmiller, B., Aebersold, R., Simons, K., Shevchenko, A., Ejsing, C. S., and Weissman, J. S. (2010). Orm family proteins mediate sphingolipid homeostasis. Nature *463*, 1048–1053.

Casamayor, A., Torrance, P. D., Kobayashi, T., Thorner, J., and Alessi, D. R. (1999). Functional counterparts of mammalian protein kinases PDK1 and SGK in budding yeast. Curr. Biol. *9*, 186–197.

Enciso, G., Kellogg, D. R., and Vargas, A. (2014). Compact modeling of allosteric multisite proteins: application to a cell size checkpoint. PLoS Comput Biol *10*, e1003443.

Friant, S., Lombardi, R., Schmelzle, T., Hall, M. N., and Riezman, H. (2001). Sphingoid base signaling via Pkh kinases is required for endocytosis in yeast. Embo J *20*, 6783–6792.

Friant, S., Zanolari, B., and Riezman, H. (2000). Increased protein kinase or decreased PP2A activity bypasses sphingoid base requirement in endocytosis. Embo J *19*, 2834–2844.

Hua, Z., Fatheddin, P., and Graham, T. R. (2002). An essential subfamily of Drs2p-related P-type ATPases is required for protein trafficking between Golgi complex and endosomal/vacuolar system. Mol. Biol. Cell *13*, 3162–3177.

Inagaki, M., Schmelzle, T., Yamaguchi, K., Irie, K., Hall, M. N., and Matsumoto, K. (1999). PDK1 homologs activate the Pkc1-mitogen-activated protein kinase pathway in yeast. Molecular and Cellular Biology *19*, 8344–8352.

Janke, C. *et al.* (2004). A versatile toolbox for PCR-based tagging of yeast genes: new fluorescent proteins, more markers and promoter substitution cassettes. Yeast *21*, 947–962.

Kamada, Y., Fujioka, Y., Suzuki, N. N., Inagaki, F., Wullschleger, S., Loewith, R., Hall, M. N., and Ohsumi, Y. (2005). Tor2 Directly Phosphorylates the AGC Kinase Ypk2 To Regulate Actin Polarization. Molecular and Cellular Biology *25*, 7239–7248.

Kamada, Y., Qadota, H., Python, C. P., Anraku, Y., Ohya, Y., and Levin, D. E. (1996). Activation of yeast protein kinase C by Rho1 GTPase. J. Biol. Chem. *271*, 9193–9196.

Kettenbach, A. N., and Gerber, S. A. (2011). Rapid and reproducible single-stage phosphopeptide enrichment of complex peptide mixtures: application to general and phosphotyrosine-specific phosphoproteomics experiments. Anal. Chem. *83*, 7635–7644.

Klose, C., Surma, M. A., Gerl, M. J., Meyenhofer, F., Shevchenko, A., and Simons, K. (2012). Flexibility of a eukaryotic lipidome--insights from yeast lipidomics. PLoS ONE *7*, e35063.

Lew, D. J., and Reed, S. I. (1993). Morphogenesis in the yeast cell cycle: regulation by Cdc28 and cyclins. The Journal of Cell Biology *120*, 1305–1320.

Li, Y., Moir, R. D., Sethy-Coraci, I. K., Warner, J. R., and Willis, I. M. (2000). Repression of Ribosome and tRNA Synthesis in Secretion-Defective Cells Is Signaled by a Novel Branch of the Cell Integrity Pathway. Molecular and Cellular Biology *20*, 3843–3851.

Liu, K., Zhang, X., Lester, R. L., and Dickson, R. C. (2005). The Sphingoid Long Chain Base Phytosphingosine Activates AGC-type Protein Kinases in Saccharomyces cerevisiae Including Ypk1, Ypk2, and Sch9. Journal of Biological Chemistry *280*, 22679–22687.

Longtine, M. S., McKenzie, A., DeMarini, D. J., Shah, N. G., Wach, A., Brachat, A., Philippsen, P., and Pringle, J. R. (1998). Additional modules for versatile and economical PCR-based gene deletion and modification in Saccharomyces cerevisiae. Yeast *14*, 953–961.

McCusker, D., and Kellogg, D. R. (2012). Plasma membrane growth during the cell cycle: unsolved mysteries and recent progress. Current Opinion in Cell Biology *24*, 845–851.

Meier, K. D., Deloche, O., Kajiwara, K., Funato, K., and Riezman, H. (2006). Sphingoid base is required for translation initiation during heat stress in Saccharomyces cerevisiae. Mol. Biol. Cell *17*, 1164–1175.

Mizuta, K., and Warner, J. R. (1994). Continued functioning of the secretory pathway is essential for ribosome synthesis. Molecular and Cellular Biology *14*, 2493–2502.

Nakano, K., Yamamoto, T., Kishimoto, T., Noji, T., and Tanaka, K. (2008). Protein kinases Fpk1p and Fpk2p are novel regulators of phospholipid asymmetry. Mol. Biol. Cell *19*, 1783–1797.

Nanduri, J., and Tartakoff, A. M. (2001). The arrest of secretion response in yeast: signaling from the secretory path to the nucleus via Wsc proteins and Pkc1p. Molecular Cell *8*, 281–289.

Nonaka, H., Tanaka, K., Hirano, H., Fujiwara, T., Kohno, H., Umikawa, M., Mino, A., and Takai, Y. (1995). A downstream target of RHO1 small GTP-binding protein is PKC1, a homolog of protein kinase C, which leads to activation of the MAP kinase cascade in Saccharomyces cerevisiae. Embo J *14*, 5931–5938.

Pichler, H., Gaigg, B., Hrastnik, C., Achleitner, G., Kohlwein, S. D., Zellnig, G., Perktold, A., and Daum, G. (2001). A subfraction of the yeast endoplasmic reticulum associates with the plasma membrane and has a high capacity to synthesize lipids. Eur. J. Biochem. *268*, 2351–2361.

Pomorski, T., Lombardi, R., Riezman, H., Devaux, P. F., van Meer, G., and Holthuis, J. C. M. (2003). Drs2p-related P-type ATPases Dnf1p and Dnf2p are required for phospholipid translocation across the yeast plasma membrane and serve a role in endocytosis. Mol. Biol. Cell *14*, 1240–1254.

Roelants, F. M., Baltz, A. G., Trott, A. E., Fereres, S., and Thorner, J. (2010). A protein kinase

network regulates the function of aminophospholipid flippases. Proc. Natl. Acad. Sci. U.S.a. *107*, 34–39.

Roelants, F. M., Breslow, D. K., Muir, A., Weissman, J. S., and Thorner, J. (2011). Protein kinase Ypk1 phosphorylates regulatory proteins Orm1 and Orm2 to control sphingolipid homeostasis in Saccharomyces cerevisiae. Proc. Natl. Acad. Sci. U.S.a. *108*, 19222–19227.

Roelants, F. M., Torrance, P. D., and Thorner, J. (2004). Differential roles of PDK1- and PDK2-phosphorylation sites in the yeast AGC kinases Ypk1, Pkc1 and Sch9. Microbiology (Reading, Engl.) *150*, 3289–3304.

Roelants, F. M., Torrance, P. D., Bezman, N., and Thorner, J. (2002). Pkh1 and Pkh2 differentially phosphorylate and activate Ypk1 and Ykr2 and define protein kinase modules required for maintenance of cell wall integrity. Mol. Biol. Cell *13*, 3005–3028.

Rossio, V., and Yoshida, S. (2011). Spatial regulation of Cdc55-PP2A by Zds1/Zds2 controls mitotic entry and mitotic exit in budding yeast. The Journal of Cell Biology *193*, 445–454.

Schmelzle, T., Helliwell, S. B., and Hall, M. N. (2002). Yeast Protein Kinases and the RHO1 Exchange Factor TUS1 Are Novel Components of the Cell Integrity Pathway in Yeast. Molecular and Cellular Biology *22*, 1329–1339.

Sun, Y., Miao, Y., Yamane, Y., Zhang, C., Shokat, K. M., Takematsu, H., Kozutsumi, Y., and Drubin, D. G. (2012). Orm protein phosphoregulation mediates transient sphingolipid biosynthesis response to heat stress via the Pkh-Ypk and Cdc55-PP2A pathways. Mol. Biol. Cell *23*, 2388–2398.

Sun, Y., Taniguchi, R., Tanoue, D., Yamaji, T., Takematsu, H., Mori, K., Fujita, T., Kawasaki, T., and Kozutsumi, Y. (2000). Sli2 (Ypk1), a homologue of mammalian protein kinase SGK, is a downstream kinase in the sphingolipid-mediated signaling pathway of yeast. Molecular and Cellular Biology *20*, 4411–4419.

Villén, J., and Gygi, S. P. (2008). The SCX/IMAC enrichment approach for global phosphorylation analysis by mass spectrometry. Nat Protoc *3*, 1630–1638.

Wullschleger, S., Loewith, R., Oppliger, W., and Hall, M. N. (2005). Molecular organization of target of rapamycin complex 2. J. Biol. Chem. *280*, 30697–30704.

Yamochi, W., Tanaka, K., Nonaka, H., Maeda, A., Musha, T., and Takai, Y. (1994). Growth site localization of Rho1 small GTP-binding protein and its involvement in bud formation in Saccharomyces cerevisiae. The Journal of Cell Biology *125*, 1077–1093.

List of Tables

Table S1.

All identified phosphorylation sites.

Table S2.
All identified phosphopeptides.

Table S3.
Sites that show a significant decrease in phosphorylation in response to an arrest of membrane growth.

Table S4.
Sites that show a significant increase in phosphorylation in response to an arrest of membrane growth.

Table S5.
Yeast strains used in this study.

Table S5. Yeast Strains

Strain	Genotype	Background	Reference
DK186	MATa *bar-*	W303	Altman and Kellogg, 1997
DK1475	MATa bar- *sec6-4::kanMX*	W303	Anastasia et al. 2012
DK2112	MATa bar- *CUP1-PKC1*::URA3*	W303	Anastasia et al. 2012
DK2517	MATa bar- YPK1-6xHA::URA4 sec6-4::kanMX	W303	This study
DK2547	MATa *PKH1-as(L203A F187V) pkh2::LEU2*	W303	This study
DK2812	MATa bar- YPK1-6xHA::URA3	W303	This study
DK2876	MATa bar- *YPK1-as(L424A) ypk2::HIS3*	W303	This study
DK2987	MATa bar- *YPK1-as(L424A) ypk2::HIS3 CUP1-PKC1*::URA3*	W303	This study
DK3018	MATa bar- *3xFLAG-ORM2::natNT2*	W303	This study
DK3050	MATa bar- *3xFLAG-ORM2::natNT3 sec6-4::kanMX*	W303	This study
DDY903	MATa	S288C	Gift of Y. Sun and D. Drubin
YSY1269	MATa *lcb1-100*	S288C	Gift of Y. Sun and D. Drubin

Figure 1

Blocking membrane traffic causes reduced sphingolipid-dependent signaling.

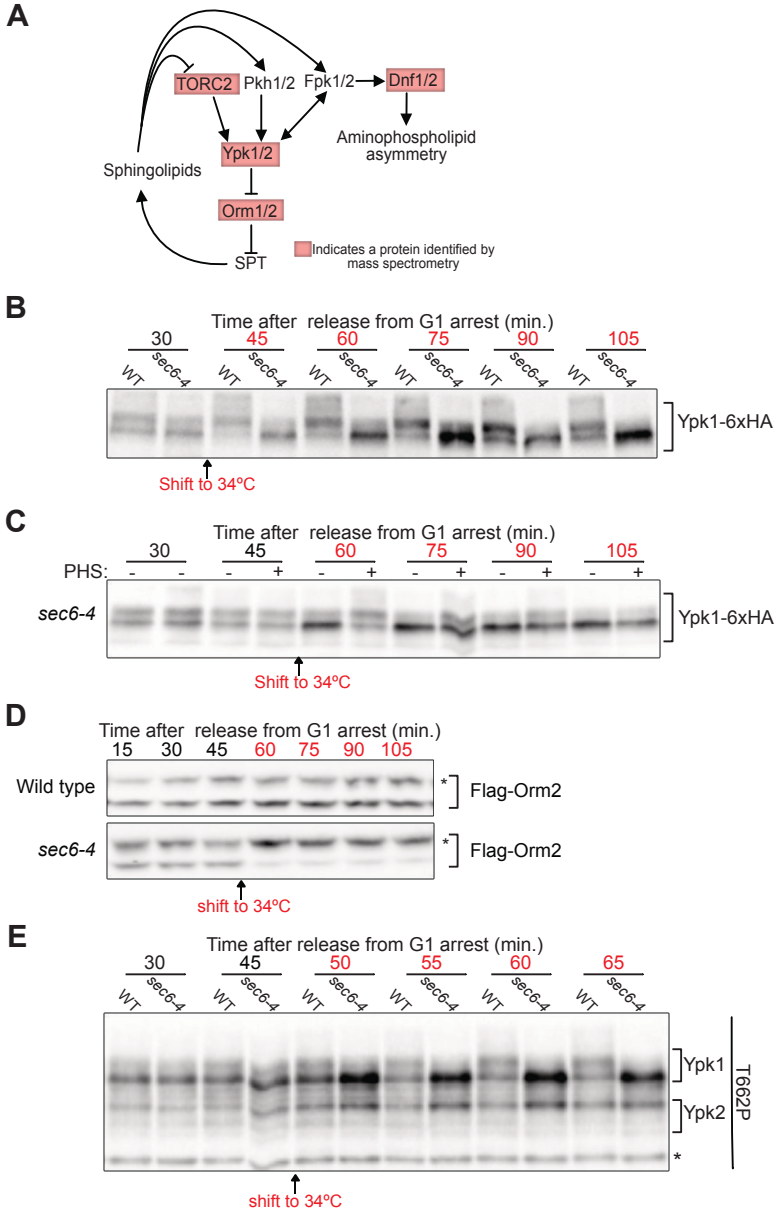

Figure 1. (**A**) Proteins in the network that showed a major change in phosphorylation upon growth arrest are highlighted in red. (**B**) *YPK1-6xHA* cells with or without the *sec6-4* allele were released from G1 arrest at 22°C and shifted to 34°C after 30 minutes. Ypk1-6xHA phosphorylation was assayed by western blot. (**C**) *YPK1-6xHA sec6-4* cells were released from G1 arrest at 22°C and shifted to 34°C after 45 minutes. 10 μM phytosphingosine was added to one half of the culture (+) immediately after the shift to 34°C. Ypk1 phosphorylation was assayed by western blot. (**D**) *Flag-ORM2* cells with or without the *sec6-4* allele were released from G1 arrest at 22°C and shifted to 34°C after the 45 minute time point. Flag-Orm2 phosphorylation (*) was assayed by running samples on a Phos-Tag™ gel followed by western blot. (**E**) Cells with or without the *sec6-4* allele were released from G1 arrest at 22°C and shifted to 34°C after 45 minutes. TORC2-dependent phosphorylation of Ypk1-T662P was assayed by western blot with a phospho-specific polyclonal antibody that recognizes TORC2 sites on Ypk1 and Ypk2. A non-specific background band that serves as a loading control is marked with an asterisk.

Figure 2

Pkc1 phosphorylation is dependent upon Ypk1/2 activity.

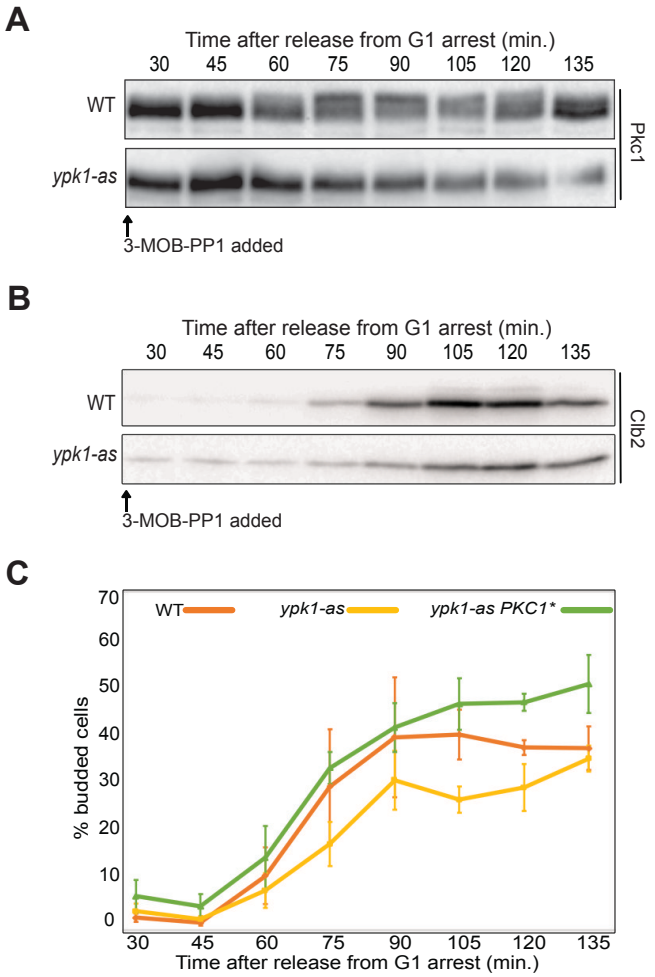

Figure 2. (**A**) The indicated cells were released from a G1 arrest at 25°C and 50 μM 3-MOB-PP1 was added to each strain at 10 min after release. Pkc1 phosphorylation was assayed by western blot. (**B**) A western blot showing levels of Clb2 protein in the same samples as panel A. (**C**) Cells were released from a G1 arrest at 25°C and 50μM 3-MOB-PP1 was added at 10 min after release. The percentage of budded cells was determined by counting the number of budded cells in a total of at least 200 cells for each time point. The percentage of budded cells was averaged for three biological replicates. Error bars represent the standard error of the mean for three biological replicates.

Figure 3

Inactivation of Ypk1/2 causes a failure in Pkc1 phosphorylation and prolonged polar growth.

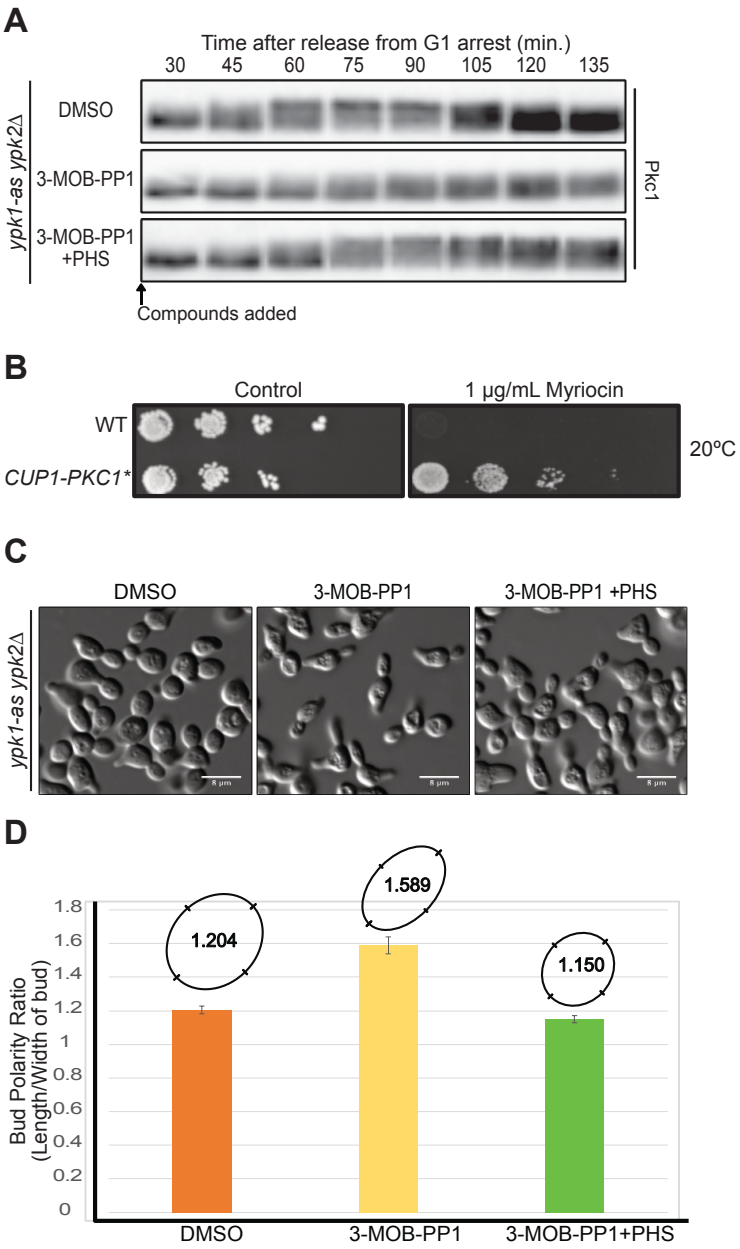

Figure 3. (**A**) *ypk1-as ypk2Δ* cells were released from a G1 arrest at 25°C and the indicated compounds were added at 10 min after release. Pkc1 phosphorylation was assayed by western blot. (**B**) 10-fold serial dilutions of wild type and *CUP1-PKC1** cells were spotted on YPD control plates or plates containing 1 µg/mL myriocin. Plates were grown at 22°C and imaged after 2 days of growth. (**C**) Fixed cells from the 120 minute time point of panel A were imaged by DIC microscopy. (**D**) Bud polarity of the imaged cells in panel B were determined by calculating the ratio of the bud length to width of buds for 50 cells and then plotting the average ratio. Error bars represent the standard error of the mean. The average polarity ratios were also converted to ovals whose shape can be directly compared.

Figure 4

Pkh1/2 are not required for Pkc1 hyperphosphorylation and exogenous phytosphingosine can not induce Pkc1 phosphorylation in *sec6-4* cells.

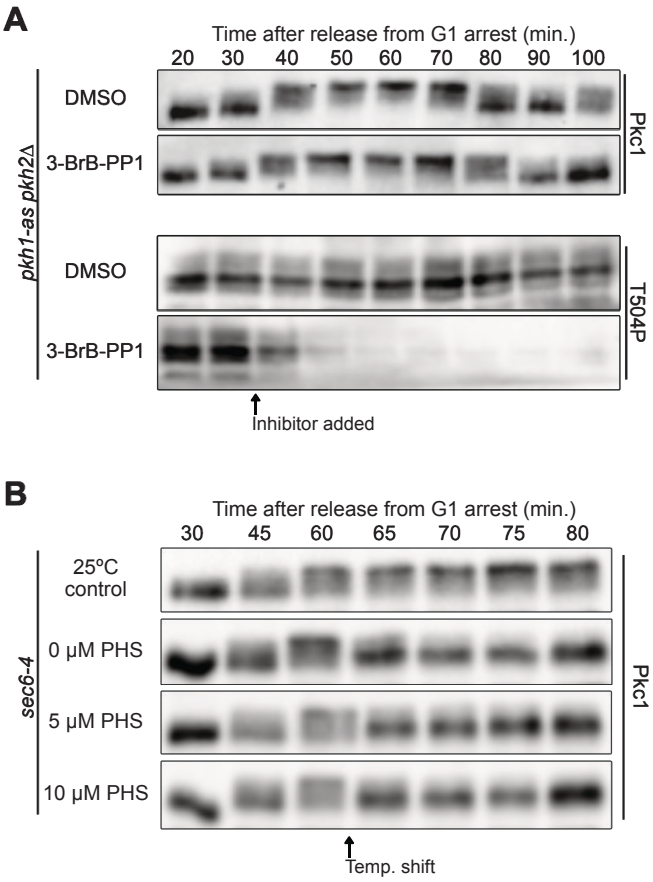

Figure 4. (**A**) *pkh1-as pkh2Δ* were released from a G1 arrest and DMSO or 15 μM 3-BrB-PP1 were added at 30 min after release. Pkc1 phosphorylation was assayed by western blot. Pkh1/2-dependent phosphorylation of Ypk1-T504 was assayed by western blot using a phosphospecific antibody. Blots are from the same samples so timing can be directly compared. (**B**) *sec6-4* cells were released from a G1 arrest at 25°C. At 60 minutes one 3/4 of the culture was shifted to 34°C and the indicated amounts of phytosphingosine were added. Pkc1 phosphorylation was assayed by western blot.

Figure 5

Reduced sphingolipid synthesis causes delays in Pkc1 phosphorylation and mitotic entry.

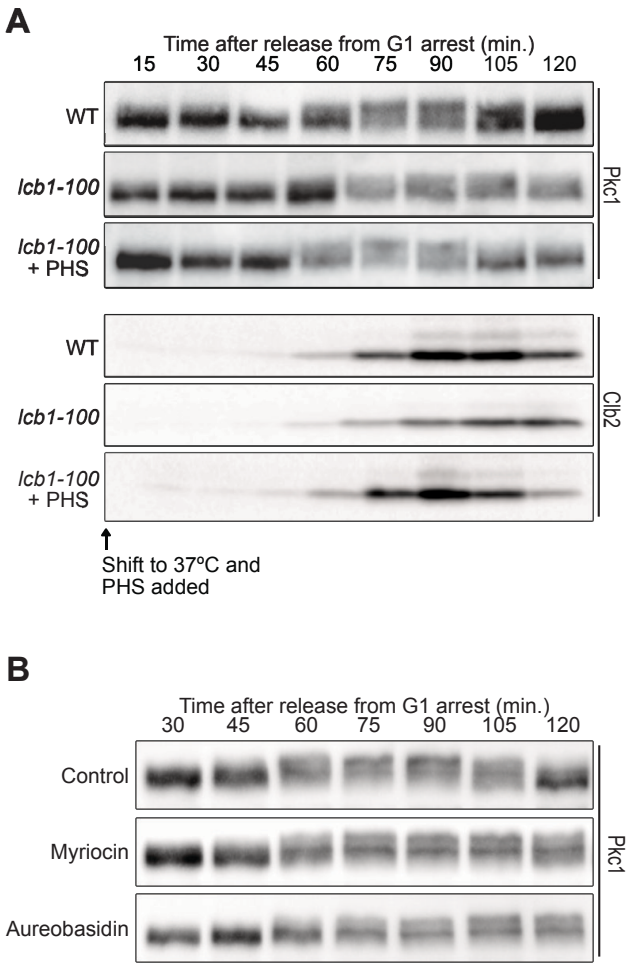

Figure 5. (**A**) Wild type and *lcb1-100* cells were arrested in G1 at 30°C and released into media at restrictive temperature (37°C) and 10 μM phytosphingosine was added 10 minutes after release from the arrest. Pkc1 phosphorylation and Clb2 protein levels were assayed by western blot. (**B**) Wild type cells were released from a G1 arrest at 23°C. Methanol (control), 0.5 μg/ml myriocin, or 0.8 μg/ml aureobasidin were added 30 minutes prior to release from G1 arrest. Cells were released from G1 in the continued presence of compounds and Pkc1 phosphorylation was assayed by western blot.

Figure Supplement 1

ATP analog 3-MOB-PP1 has no effect on wild type bud morphology.

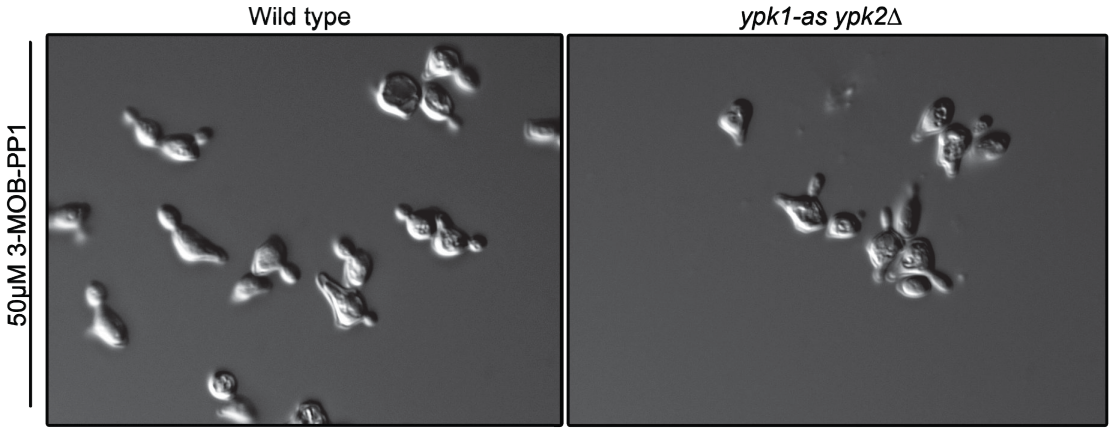

Figure supplement 1. Wild type and *ypk1-as ypk2Δ* cells were released from a G1 arrest and 50 μM 3-MOB-PP1 inhibitor was added at 10 minutes. Cells at the 120 minute time point were fixed and imaged by DIC microscopy.